Research Report

Reactively Steered Ring Antenna Array for Automotive Application

Shinya Sugiura and Hideo Iizuka

Report received on Nov. 17, 2010

ABSTRACT A novel type of smart antenna, called a reactively steered ring antenna array (RSRAA), is proposed. The antenna features a conformal configuration with three overlapping one-wavelength ring elements. Directivity can be controlled by changing the values of variable reactance circuits that are embedded in the antenna. The antenna can be mounted on the windshield of an automobile without interfering with the view of the driver. An equivalent model of six dipole elements is derived from the original antenna configuration to enable simple calculation of directivity when a set of reactance values is given. The validity of the proposed equivalent model is confirmed by comparing simulation results calculated by the equivalent model and by the method of moments. Another simulation shows that the conventional reactance domain multiple signal classification algorithm can be applied to the proposed antenna while keeping the estimated direction-of-arrival number equal to the number of reactance circuits. In addition, the characteristics of an RSRAA, which is optimized at 2.4 GHz and is mounted on an automobile, are measured in an anechoic chamber, and directivity control is found to be implemented effectively.

KEYWORDS Active antennas, Antenna arrays, Direction of arrival estimation, Road vehicles, Varactors

1. Introduction

Recently, the demand for safety applications capable of drastically reducing the number of traffic accidents has increased. Radar systems and/or imaging sensor systems have been developed for practical use. These systems are highly effective for preventing possible collisions with forward obstacles that are within the line of sight (LOS) of the incident vehicle.

However, the systems cannot work in the case of accidents that occur outside of the LOS, which accounts for a large percentage of traffic accidents in Japan. To solve this problem, safety applications using wireless communication, such as intervehicle communication (IVC), are presently being studied extensively.[1-3] As IVC is categorized as a high-mobile ad hoc network, space-division multiple access by smart antennas can be applied for the purpose of increasing system capacity and gain.[4] Dedicated short-range communications (DSRCs) have already been used in commercial applications in addition to safety applications. Smart antennas can also be used for sharing system resources between DSRC and IVC.[5]

Many types of smart antennas have been designed. Digital beamforming (DBF) antennas are typical examples of high performance antennas, but these antennas have major disadvantages with respect to cost and size. This is a result of the requirement for DBF antennas to have multiple antenna elements and the same number of radio-frequency (RF) chains, including low-noise amplifiers (LNAs), downconverters, and analog-to-digital converters. In essence, vehicle safety applications are applied in all types of vehicles, i.e., not only expensive vehicles but also popular types of vehicles. Therefore, smart antennas must be low-cost. To realize a simpler configuration of smart antennas, various types of analog beamforming (ABF) antennas have been developed. Typical examples include reactively steered antennas, which have only one active element with an RF chain and multiple parasitic elements terminated by variable reactance circuits.[6-11] By changing the values of these reactance circuits, directivity can be controlled. Here, the key point is that the antenna actively utilizes sufficient mutual couplings among the active element and the parasitic elements.

From a practical viewpoint with respect to antenna installation on automobiles, on-glass antennas are generally preferred because they do not degrade the appearance of the vehicle. In addition, considering the fact that approximately 20 antennas are installed inside the vehicle, on-glass antennas are desirable in order to save installation space. However, there are difficulties in realizing a conformal type ABF antenna that can be installed on the windshield. This is mainly because previous research has primarily focused on three-dimensional ABF antennas.[6,8,9] With regard to the microstrip type ABF antenna,[7] it is difficult to design an on-glass antenna because of the ground plate. It is possible to achieve a conformal configuration by reducing the number of parasitic elements to two in previous work,[6,8,9] but this has the effect of degrading beamforming performance. In addition, this leads to lower performance with respect to other capabilities, such as direction-of-arrival (DOA) estimation using the reactance domain multiple signal classification (MUSIC) algorithm.[11] The maximum estimated number of DOAs is given by the number of reactance circuits that are sufficiently coupled with a feed point. Therefore, the estimated number of DOAs also decreases with the decrease in the number of effective parasitic elements in the previous study.

This paper proposes a novel type of ABF antenna, called a reactively steered ring antenna array (RSRAA). The concept of the RSRAA was originally presented in ref. (12). Further numerical and experimental studies are next described. Note that the operating frequency is chosen to be 2.4 GHz throughout this paper. The RSRAA is characterized by a conformal configuration, which maintains the number of reactance circuits that are strongly coupled with a feed point as five. The configuration and concept of the RSRAA are described in Section 2. Here, an equivalent model is also presented for the purpose of simple calculation of incident directivity when a set of reactance values is given. The performance of the RSRAA is described in Section 3. Results of parameter studies and examples of beam patterns are obtained by Monte Carlo (MC) simulation. Section 4 describes experimental results of a prototype antenna, including patterns of the antenna mounted on a windshield. A brief comment on the antenna module configuration is then presented from a practical viewpoint. An additional discussion regarding the antenna configuration is also presented. Finally, this paper is concluded in Section 5.

2. Reactively steered ring antenna array

This section presents the configuration and concept of the RSRAA.

2. 1 Configuration

A configuration of the proposed reactively steered ring antenna array is shown in **Fig. 1**(a) and (b), which shows top and side views, respectively. In addition, a mounted RSRAA on a windshield is shown in Fig. 1(c). Three overlapping ring-shaped wires are provided without any mutually nodal points. The circuit length of each of the ring wires is given by one wavelength λ. A balanced feed point and five reactance circuits are embedded in the wires. These elements are positioned along the same straight line when viewed from the x-axis. By changing the values of the

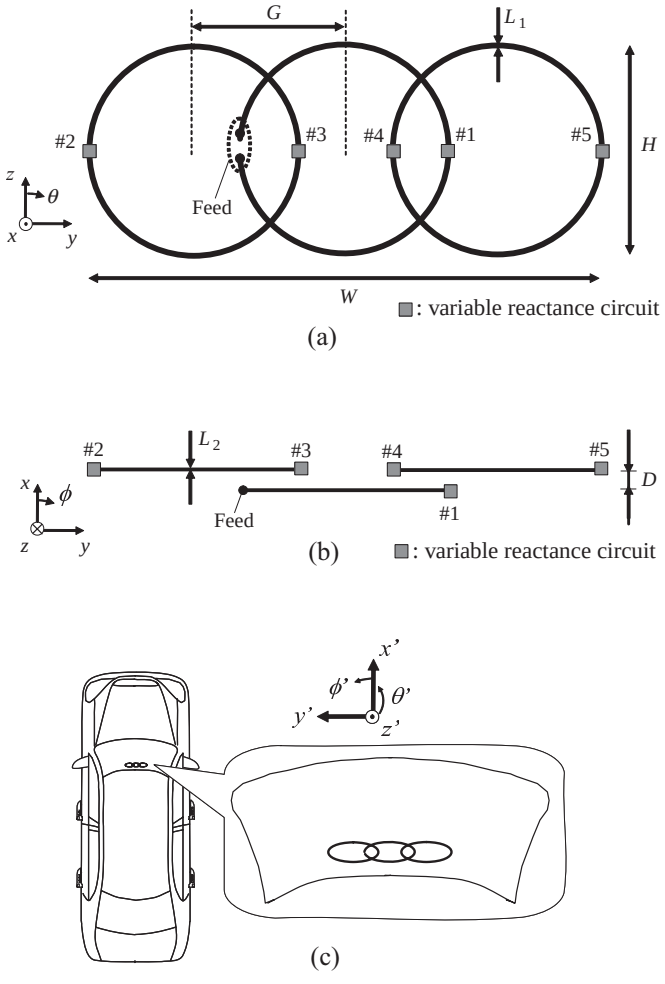

Fig. 1 Configuration of proposed antenna. Each figure shows (a) top view, (b) side view, and (c) overview of a mounted antenna on a windshield.

reactance circuits, directivity can be controlled in the *xy*-plane. In practical terms, the reactance circuits are made of chip parts such as varactor diodes, the values of which are controlled by changing their input voltages. In this way, the proposed smart antenna realizes a simple and conformal configuration.

2. 2 Equivalent model

The directivity of previous ABF antennas can be formulated as a function of values of reactance circuits.[9] The method of applying the formulation to RSRAA is given here. As described in ref. (13), a one-wavelength ring antenna is represented by two in-phase dipole antennas with a spacing of 0.27λ. This is because large current distributions are concentrated on both the feed point and the opposite point of the feed on the ring element. Using this relation, RSRAA is assumed to have an equivalent model as shown in **Fig. 2**, which is composed of six dipole elements. Accordingly, the directivity $D(\varphi, \mathbf{x})$ in the *xy*-plane is represented by a function of values of reactance circuits $\mathbf{x} = [x_1 \ldots x_5]^T$ as follows:[9]

$$D(\varphi, \mathbf{x}) = \alpha \boldsymbol{w}(\mathbf{x})^T \boldsymbol{a}(\varphi)^T \cdots\cdots (1)$$

where α is a constant, and the weight vector $\boldsymbol{w}(\mathbf{x})$ and steering vector $\boldsymbol{a}(\varphi)$ are given by

$$\boldsymbol{w}(\mathbf{x}) = (Y^{-1} + X_r)^{-1} \boldsymbol{u}_0 \cdots\cdots (2)$$

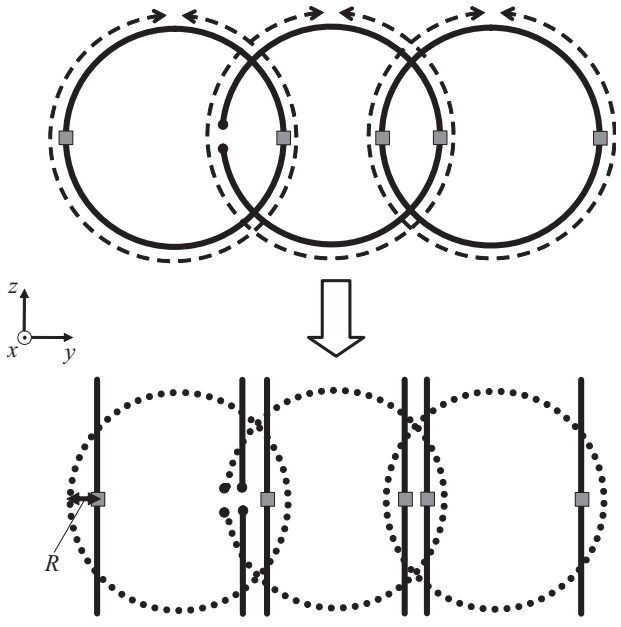

Fig. 2 Equivalent model of RSRAA. The model is composed of a dipole element array.

$$\boldsymbol{a}(\varphi) = \left[\exp\left\{ j \frac{2\pi}{\lambda} \boldsymbol{r}_0^T \boldsymbol{L}(\varphi) \right\} \cdots \exp\left\{ j \frac{2\pi}{\lambda} \boldsymbol{r}_5^T \boldsymbol{L}(\varphi) \right\} \right]^T \cdots\cdots (3)$$

respectively, where

$$X_r = \mathrm{diag}[z_s \ j\mathbf{x}^T] \cdots\cdots (4)$$

$$\boldsymbol{u}_0 = [1 \ 0 \ 0 \ 0 \ 0 \ 0]^T \cdots\cdots (5)$$

$$\boldsymbol{L}(\varphi) = [\cos\varphi \ \ \sin\varphi \ \ 0]^T. \cdots\cdots (6)$$

Here, components of the admittance matrix Y are mutual admittances among the ports (the feed point and the five reactance circuits). Position vectors r_i (i = 0,⋯,5) represent the positions of the feed (i = 0) and the reactance circuits (i = 1⋯5) in the equivalent model, respectively. In addition, z_s is the characteristic impedance. From the equivalent model, the antenna is found to be polarized vertically. Note that Y has to be calculated by full-wave simulations before applying the formulated directivity (1), as noted in ref. (9). In general, reactively steered types of smart antennas actively utilize mutual couplings among elements.[6] The RSRAA realizes strong mutual coupling among each port because the ring wires are overlapping and share magnetic fields through the areas. It should be noted that these strong mutual couplings of the RSRAA cannot be obtained by a real dipole array that is identical to the array of the equivalent model.

3. Performance

In this section, numerical analysis is carried out in order to clarify the performance of the RSRAA. First, beamforming abilities were examined by a MC simulation. The conventional reactance domain MUSIC algorithm[11] was then applied to the RSRAA for estimating DOAs at a high resolution. Admittance matrix Y, as well as radiation properties of the antenna, are calculated in free space using commercial simulator "FEKO" based on the method of moments (MoM). Note that reactance values are assumed to be excluded in the case of Y calculation. The basic parameters of the antenna configuration are shown in **Table 1**. Unless otherwise noted, these parameters are used throughout this paper.

3. 1 Parameter study

The dependence of the antenna gain on the beam direction was calculated. **Figure 3** shows the gain toward each direction at every 10° from $\varphi = -90°$ to $\varphi = 90°$ with $\theta = 90°$. Here, each of the simulated gains

$G_n(\varphi, \mathbf{x})$ is normalized in the horizontal plane, which is given by the following:

$$G_n(\varphi, \mathbf{x}) = \frac{D(\varphi, \mathbf{x})}{\int_{-\pi/2}^{\pi/2} D(\varphi', \mathbf{x}) d\varphi'} \quad \cdots\cdots\cdots\cdots\cdots (7)$$

In order to determine each beam pattern $G_n(\varphi, \mathbf{x})$, 100 000 random sets of $\mathbf{x}$ were generated. Here, directivity $D(\varphi, \mathbf{x})$ in (1) was chosen as the cost function to be maximized for each φ. The following three cases were selected as the simulation conditions of the variable range of each reactance value: (x_m, x_M)=(−50 Ω, 0 Ω),(−100 Ω, 0 Ω), and (−150 Ω, 0 Ω), where x_m and x_M are minimum and maximum values of the variable range, respectively. First, it was found that beamforming ability differs depending on direction. In the case of (−150 Ω, 0 Ω), for example, the maximum normalized gain reaches 5 dB at $\varphi = 0^o$. On the other hand, the normalized gains toward the directions of approximately $\varphi = 30^o$ and -45^o are lower in comparison with the average. Secondly, the calculated gain is greatly influenced by the range of variable reactance values. As shown in the figure, the case of the narrowest reactance range, i.e., (x_m, x_M) = (−50 Ω, 0 Ω), shows a much lower performance than the other two cases. The range of the variable reactance circuits must be higher than a certain value. Next, the influence of the spacing G between the centers of the closest ring elements on the beamforming ability was examined. The simulation results are shown in **Fig. 4**. Here, the average gain in the figure is defined by averaging the calculated normalized gain in (7) for each direction. Parameters other than G were kept constant, and the range of the reactance values was set to (x_m, x_M) = (−150 Ω, 0 Ω). The figure shows that the beamforming ability is highest when $G = \lambda/4$. Thus, G was set to $\lambda/4$.

Table 1 Parameters of calculated model.

Height H of the antenna	39.8 mm ($= \lambda/\pi$)
Length D	0.125 mm
Length G	312.5 mm ($= \lambda/4$)
Line width L_1	1.5 mm
Line height L_2	0.03 mm

3. 2 Beamforming

Figure 5 shows beam patterns toward $\varphi = -90^o$, -30^o, 0^o, 30^o and 90^o, each of which is calculated by both MoM and the equivalent model represented by (1). In terms of MoM simulations, the values of the reactance circuits are built into the model as lumped-parameter elements. Each incident $\mathbf{x}$ for each beam pattern is obtained by MC simulation of 100 000 random $\mathbf{x}$ in the same way as the former simulation of the parameter study. Here, (x_m, x_M) is set by (−300 Ω, 300 Ω). The reactance values obtained by MC simulation are listed in **Table 2**. Each half-power beam width (HPBW) is also described in the table. The following two findings were observed in the simulation results. First, typical beam patterns toward the desired directions were formed. Thus, an effective beam control technique was verified by calculation.

Note that, in the simulated cases, HPBW changes from 45^o to 93^o, depending on the beam direction. This is because the equivalent array works as a broad side array at $\varphi = 0^o$ and as an end-fire array at $\varphi = \pm 90^o$. Secondly, the patterns by MoM and the equivalent model are quite similar especially around the direction of the beam. Therefore, the fundamental validity of the

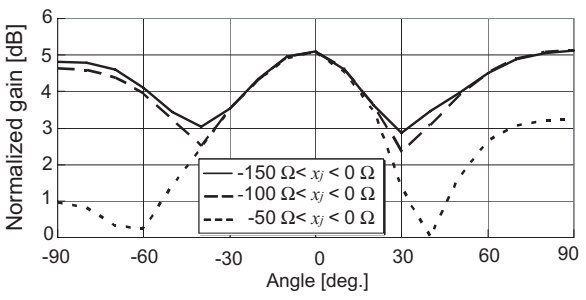

Fig. 3 Dependence of variable range of reactance values on beamforming toward each direction in the case of (x_m, x_M) = (−50 Ω, 0 Ω), (−100 Ω, 0 Ω), and (−150 Ω, 0 Ω), respectively.

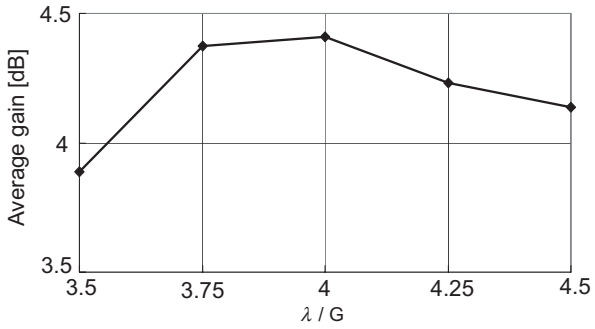

Fig. 4 Calculated average gain of each direction for parameter study in the case of $G = \lambda/3.5$, $\lambda/3.75$, $\lambda/4$, $\lambda/4.25$, and $\lambda/4.5$.

proposed equivalent model was confirmed. On the other hand, slight differences are found at the sidelobes and the nulls. These may be caused by a model error of the equivalent model, such as positions of the equivalent dipoles and/or their resonance amplitudes and phases.

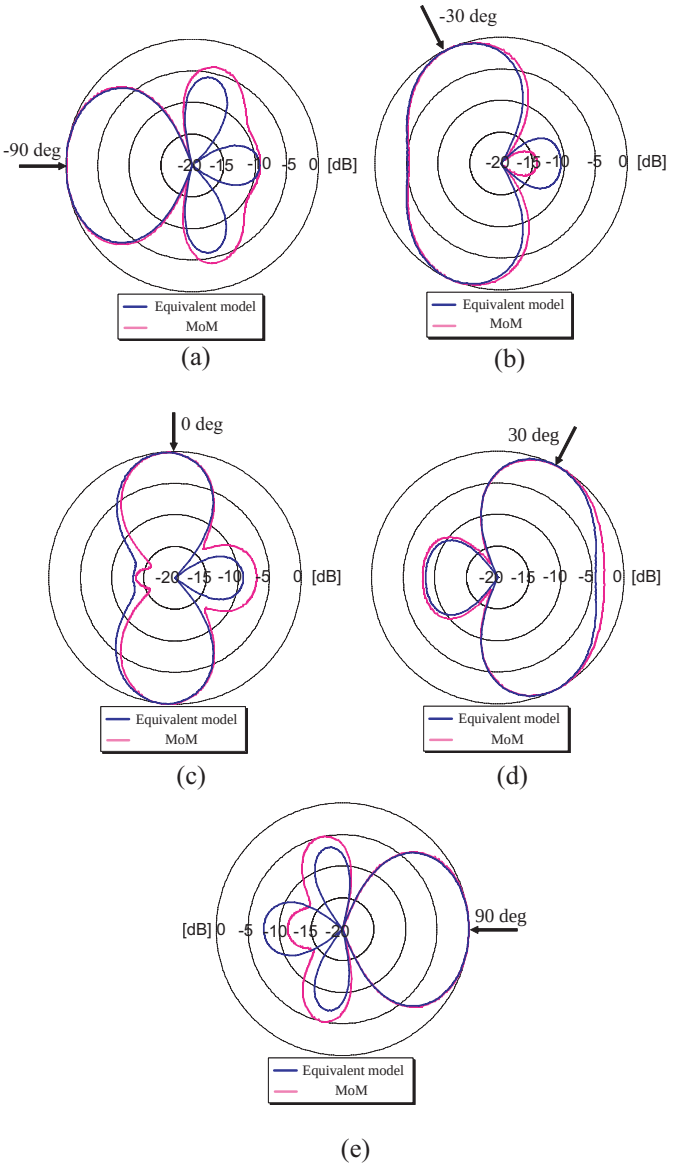

Fig. 5 Comparison between patterns calculated by equivalent model and by MoM. (a) −90°, (b) −30°, (c) 0°, (d) 30°, and (e) 90°.

3. 3 MUSIC

Another capability of the proposed antenna, i.e., DOA estimation, is presented here. As described in Section 2, the equivalent model enables the steering vector to be defined, as represented in (3). Using this steering vector, the conventional reactance domain MUSIC algorithm[11] was applied to the proposed antenna, and its performance was verified numerically. The simulation parameters are listed in **Table 3**. Here, three uncorrelated waves are assumed, and the signal-to-noise ratio (SNR) of each of the waves is given as 20 dB. **Figure 6** shows the simulation results of MUSIC. It was found that DOAs can be estimated at a high resolution and with estimated errors of less than

Table 3 Simulation parameters for MUSIC.

Number of Waves	3 (uncorrelated)
DOAs	−60 deg, 0 deg, 45 deg
SNR	20 dB (each of the waves)

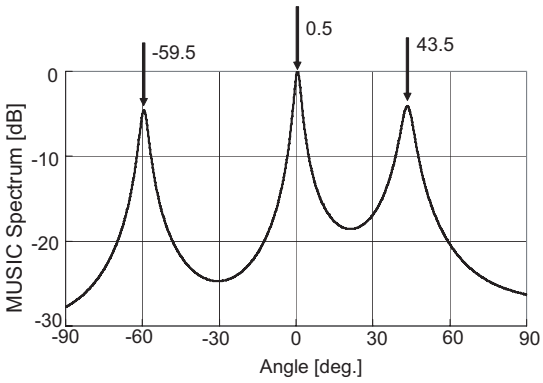

Fig. 6 Calculated MUSIC spectrum for a set of reactance values. DOAs = −60°, 0°, and 45°. SNR = 20 dB for each signal.

Table 2 Incident values of reactance circuits used in pattern simulation.

Direction	x_1	x_2	x_3	x_4	x_5	HPBW
−90 deg	−157.3 Ω	106.2 Ω	−168.4 Ω	−153.2 Ω	162.4 Ω	93 deg
−30 deg	36.3 Ω	156.0 Ω	34.5 Ω	268.6 Ω	295.3 Ω	64 deg
0 deg	−63.1 Ω	−17.5 Ω	7.8 Ω	−64.9 Ω	−79.5 Ω	45 deg
30 deg	−122.2 Ω	56.9 Ω	193.0 Ω	9.7 Ω	−229.2 Ω	57 deg
90 deg	−49.0 Ω	39.1 Ω	−107.8 Ω	−123.2 Ω	24.7 Ω	92 deg

0.5°. Note that the proposed antenna can estimate a maximum of five DOAs. As shown in ref. (11), this maximum number is equal to the number of variable reactance circuits. On the other hand, in a real dipole array, the configuration of which corresponds to the equivalent model of the proposed antenna, a maximum of only two DOAs can be estimated. This is because the active element couples with only the closest parasitic elements in such a real dipole array. Thus, the proposed antenna has the advantage of the ability to estimate many more DOAs than the conventional dipole array in the conformal configuration.

4. Experiment

4. 1 Prototype antenna

A prototype antenna was constructed on a typical Teflon substrate with a thickness H of 0.6 mm and a dielectric constant ε_r of 2.6. Here, the configured parameters of the prototype antenna are the same as those listed in Table 1, except for $H = 0.6$ mm. Copper was etched on both sides of the substrate, and reactance circuits were mounted using chip parts (varactors, capacitors, and resistors). The equivalent circuit of the reactance circuits is shown in **Fig. 7**. The main components of the circuit are a serial varactor and a blocking capacitor. The varactor is DC biased through choke resistors of 10 kΩ. The bias lines are drawn orthogonally to the polarization in order not to affect the radiation pattern. The feed point is connected to a parallel line, the characteristic impedance of which is 200 Ω. The width of each line and the distance between the centers of the two lines were chosen to be 1.6 mm and 3.0 mm, respectively. The end of the parallel line is connected to an LC balun, which transforms the 200 Ω balanced line to a 50 Ω unbalanced line. The measured insertion loss of the LC balun is 0.29 dB at 2.4 GHz. **Figure 8** shows the patterns that were measured in an anechoic chamber and calculated using MoM. Here, Fig. 8(a) and (b) represents the beam patterns toward 10° and 30°, respectively. The incident sets of reactance values are also listed in **Table 4**. Here, in order to obtain these values, MC simulations were conducted in the same way as in Section 3. Based on these results, the measured patterns and simulated patterns were found to be quite similar.

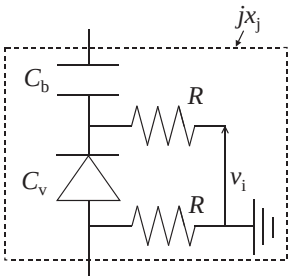

Fig. 7 Equivalent circuit model of variable reactance circuit.

4. 2 Mounted antenna

The prototype antenna was mounted at the upper center region of the windshield, as shown in Fig. 1(c). The distance between the metal-top roof and the nearest side of the prototype antenna was set to be 40 mm. The angle between the windshield and the horizontal plane was approximately 30°. **Figure 9** shows the beam patterns of the mounted antenna toward $\varphi' = 10°$ and $\varphi' = 30°$ in the coordinate system shown in Fig. 1(c). In each of the cases, three patterns at every 10° of elevation angle from $\theta' = 90°$ to $\theta' = 70°$ are plotted. Here, the incident reactance values are the same as the cases shown in Fig. 8. The voltage standing-wave ratio (VSWR) with the 10° and 30° beams are 1.8 and 1.9, respectively. The measured

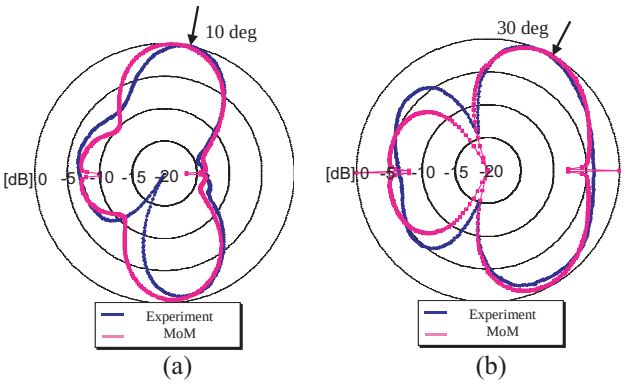

Fig. 8 Comparison between patterns measured in anechoic chamber and calculated by MoM. (a) 10° and (b) 30°.

Table 4 Incident values of reactance circuits used for measured patterns.

Direction	x_1	x_2	x_3	x_4	x_5
10 deg	−51.8 Ω	−2.1 Ω	−3.4 Ω	−56.1 Ω	−83.3 Ω
30 deg	−3.7 Ω	−21.4 Ω	−37.3 Ω	−1.8 Ω	−1.6 Ω

results indicate that effective beam patterns were obtained while keeping the return loss quite low. Note that the VSWR changes depending on the values of reactance circuits and that the VSWR can be suppressed by choosing appropriate values. The ability to suppress the VSWR depends on the variable range of reactance circuits, as well as the beamforming ability.

In addition, radiation patterns in Fig. 9 are somewhat noisy, primarily because of the reflection from the vehicle body. In general, radiation patterns at 2.4 GHz are more strongly influenced than at the very high-frequency band when antennas are mounted on vehicles.

4. 3 Antenna module

We present a brief description of an antenna module that has been designed from a practical point of view. **Figure 10**(a) shows a configuration of the proposed antenna module and Fig. 10(b) shows an example of the antenna mounted on a windshield. The overall size including a voltage bias circuit is 220 × 50 mm^2. The antenna is composed of copper-etched multilayered films. The fed ring wire, as well as the other two ring wires, are situated on the independent films. The films are made of a transparent polyethylene terephthalate (PET) substrate, the thickness H of which is 125 μm. As for the reactance circuits, chip parts are mounted using conductive paste. Each of the varactors in the reactance circuit is connected to bias lines with a width of 20 μm, and is supplied with control voltage. Then, the feed point is connected to a RF connecter through a RF circuit that is surrounded by a metal box. The RF circuit in the metal box is composed of an LC balun, a filter, and an LNA, where the LNA is prepared for the case in which the antenna is used as a part of receiving system. The filter is situated such that the LNA is not saturated. At 2.4 GHz, the insertion loss of the LC balun and the filter are 0.29 and 0.46 dB, respectively, and the gain of the LNA is 6.7 dB.

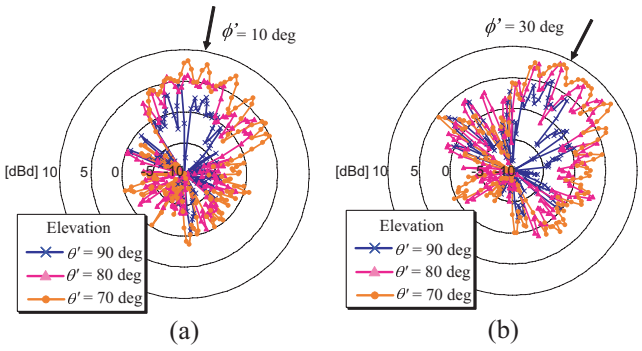

Fig. 9 Measured radiation patterns of mounted RSRAA in the φ' plane. (a) $\varphi' = 10^{o}$ and (b) $\varphi' = 30^{o}$.

4. 4 Discussion

This paper has focused on an RSRAA with three ring elements. However, the element number should be adjusted depending on the requirements of the application. For the case in which a narrower beam is required, for example, a larger number of ring elements is effective. This is because the effective length of the antenna can be increased while keeping mutual couplings among the equivalent dipoles. On the other hand, the number of reactance circuits also goes up, resulting in a more complex system. This design property has a tradeoff relationship. Furthermore, in addition to the number of ring elements, there is no

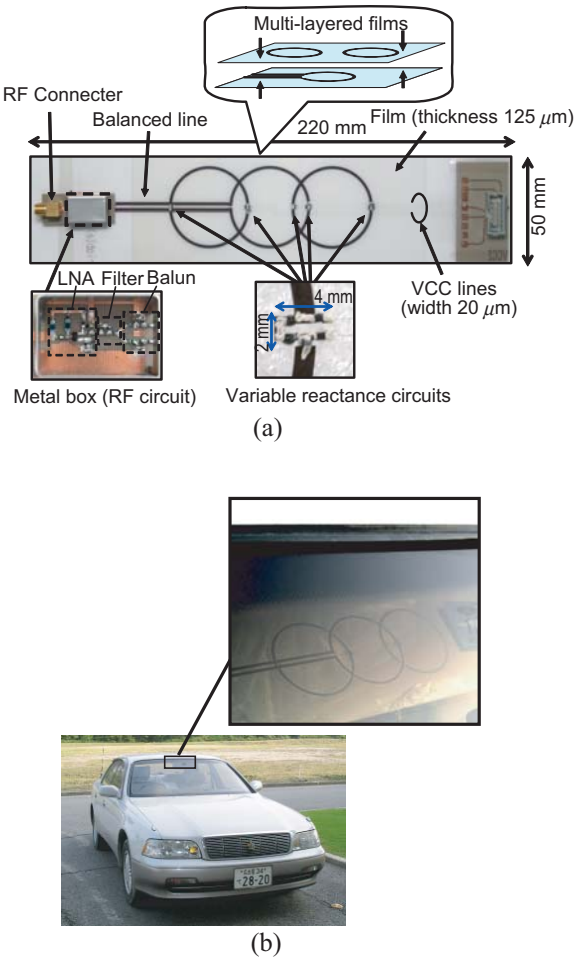

Fig. 10 Photograph of an antenna module. (a) Configuration of antenna module and (b) mounted antenna module on a windshield.

limit for the relationship among the feed and the reactance circuits. The position of the feed can be replaced by the position of one of the reactance circuits. It is important to adjust the parameters so that the performance meets the requirements of the target system.

In addition, the directivity function (1) is derived on the basis of the assumption that the circuit length of each of the ring elements is one wavelength. Thus, it is clear that the concept of the beamforming does not work when the operating frequency is out of the allowable range. A detailed consideration of the bandwidth is beyond the scope of the present paper.

5. Conclusion

A reactively steered ring antenna array and its beamforming concept have been proposed for forthcoming automotive applications. The antenna features a conformal and simple configuration composed of only one RF port with multiple variable reactance circuits. Strong mutual couplings among the feed and the reactance circuits have been realized, which contribute to beamforming performance. An equivalent dipole model was presented for simple calculation of directivity, which was verified through computer simulation. An equivalent model also enabled the conventional MUSIC algorithm to be applied to the proposed antenna. Representative beam patterns of the prototype antenna were measured for the case of $\varphi = 10^{o}$ and 30^{o} in the horizontal plane. Here, the validity was confirmed in comparison with simulation results. Furthermore, the beam patterns of the antenna mounted on the windshield of an automobile were measured, and were found to be formed effectively. Finally, brief comments on the antenna module and its settings were described. The proposed antenna will be utilized for future vehicle communications related to beamforming applications.

References

(1) Chen, W. and Cai, S., "Ad Hoc Peer-to-peer Network Architecture for Vehicle Safety Communications", *IEEE Commun. Mag.*, Vol.43, No.4 (2005), pp.100-107.
(2) Aoki, M. and Fujii, H., "Inter-vehicle Communication: Technical Issues on Vehicle Control Application", *IEEE Commun. Mag.*, Vol.34, No.10 (1996), pp.90-93.
(3) Zekavat, S. A., "A Novel Application for Wireless Communications in Vehicle Early Warning", *Proc. of IEEE Consumer Commun. Network. Conf.* (2004), pp.715-717.
(4) Tsoulos, G. V., "Smart Antennas for Mobile Communication Systems: Benefits and Challenges", *Electron. Commun. Eng. J.*, Vol.11, No.2 (1999), pp.84-94.
(5) Shimada, I., Koga, K. and Umeda, F., "Development of the Beam Control Array Antenna for DSRC and Inter-vehicle Communications", *Proc. of 11th World Congr. ITS* (2004).
(6) Harrington, R. F., "Reactively Controlled Directive Arrays", *IEEE Trans. Antennas Propag.*, Vol.26, No.3 (1978), pp.390-395.
(7) Dinger, R. J., "A Planar Version of a 4.0 GHz Reactively Steered Adaptive Array", *IEEE Trans. Antennas Propag.*, Vol.34, No.3 (1986), pp.427-431.
(8) Schlub, R., Lu, J. and Ohira, T., "Seven Element Ground Skirt Monopole ESPAR Antenna Design from a Genetic Algorithm and the Finite Element Method", *IEEE Trans. Antennas Propag.*, Vol.51, No.1 (2003), pp.3033-3039.
(9) Sun. C., Hirata, A., Ohira, T. and Karmarkar, N. C., "Fast Beamforming of Electronically Steerable Parasitic Array Radiator Antennas: Theory and Experiment", *IEEE Trans. Antennas Propag.*, Vol.52, No.7 (2004), pp.1819-1832.
(10) Lu, J., Ireland, D. and Schlub, R., "Dielectric Embedded ESPAR (DBESPAR) Antenna Array for Wireless Communication", *IEEE Trans. Antennas Propag.*, Vol.53, No.8 (2005), pp.2437-2443.
(11) Plapous, C., Cheng, J., Taillefer, E., Hirata, A. and Ohira, T., "Reactance Domain MUSIC Algorithm for Electronically Steerable Parasitic Array Radiator", *IEEE Trans. Antennas Propag.*, Vol.52, No.12 (2004), pp.3257-3264.
(12) Sugiura, S. and Iizuka, H., "Study of Reactively Steered Ring Antenna Array Suitable for Automobiles", *Proc. of IEEE AP-S Int. Symp., Albuquerque, NM* (2006), pp.2365-2368.
(13) Sawaya, K., "Review of Research and Development on Linear Antennas", *IEICE Trans. Commun.*, Vol.E86-B, No.3 (2003), pp.892-899.

Shinya Sugiura
Research Fields :
- Adaptive signal processing
- Wireless communications
Academic Degree : Ph.D
Academic Societies : IEEE, IEICE
Award :
- IEEE AP-S Japan Chapter Young Engineer Award, 2008

Hideo Iizuka
Research Fields :
- Microwave
- Optical engineering
Academic Degree : Dr. Eng.
Academic Societies : IEEE, OSA, APS, IEICE
Award :
- IEICE Young Eng. Awards, 2001